

## Experimental Section

### Materials:

All reagents were used as received without any purification: Calcium nitrate tetrahydrate ( $\text{Ca}(\text{NO}_3)_2 \cdot 4\text{H}_2\text{O}$ , 99%), europium nitrate hexahydrate ( $\text{Eu}(\text{NO}_3)_3 \cdot 6\text{H}_2\text{O}$ , 99.9%), terbium nitrate hexahydrate ( $\text{Tb}(\text{NO}_3)_3 \cdot 6\text{H}_2\text{O}$ , 99.9%), lanthanum nitrate ( $\text{La}(\text{NO}_3)_3 \cdot 6\text{H}_2\text{O}$ , 99.99%), yttrium nitrate hexahydrate ( $\text{Y}(\text{NO}_3)_3 \cdot 6\text{H}_2\text{O}$ , 99.99%), ammonium molybdate ( $(\text{NH}_4)_6\text{Mo}_7\text{O}_{24} \cdot 4\text{H}_2\text{O}$ , 99%), ammonium metavanadate ( $\text{NH}_4\text{VO}_3$ , 99.9%), ammonium phosphate monobasic ( $\text{NH}_4\text{H}_2\text{PO}_4$ , 99%), butyric acid ( $\text{CH}_3(\text{CH}_2)_2\text{COOH}$ , 99%), and butylamine ( $\text{CH}_3(\text{CH}_2)_3\text{NH}_2$ , 99%) were purchased from Sigma-Aldrich. Polymethylmethacrylate (PMMA), polydimethylsiloxane (PDMS, Dow Corning 184). Ethanol ( $\text{CH}_3\text{CH}_2\text{OH}$ , A.R), trichloromethane ( $\text{CHCl}_3$ ,  $\geq 99\%$ ), cyclohexane ( $\text{C}_6\text{H}_{12}$ , A.R) were purchased from Sinopharm Chemical Reagent Co., Ltd. The n-Hexyl alcohol ( $\text{C}_6\text{H}_{14}\text{O}$ ,  $\geq 99\%$ ), petroleum (A.R) were purchased from Shanghai Acme Biochemical Technology Co., Ltd.

**Synthesis of  $\text{CaMoO}_4:15\%\text{Eu}^{3+}$  Nanocrystals:** Butyric acid (5 mL), butylamine (5 mL), and ethanol (60 mL) were mixed in a 200-mL glass beaker. Subsequently, 0.75 mmol  $\text{Ca}(\text{NO}_3)_2$  and 4.25 mmol  $\text{Eu}(\text{NO}_3)_3$  were dissolved in the solution under continuous magnetic stirring at room temperature. A solution of 5 mmol  $(\text{NH}_4)_6\text{Mo}_7\text{O}_{24}$  in deionized water (5 mL) was then added at room temperature. A copious white precipitate formed immediately, resulting from the formation of hydrophobic  $\text{CaMoO}_4:15\%\text{Eu}^{3+}$  nanocrystals. The white solids were collected by centrifugation and washed three times with ethanol.  $\text{CaMoO}_4$  and  $\text{CaMoO}_4:10\%\text{Tb}^{3+}$  nanocrystals were prepared using the same method.

**Synthesis of  $\text{YVO}_4$  Nanocrystals:** Butyric acid (5 mL), butylamine (5 mL), and ethanol (50 mL) were mixed in a 200-mL glass beaker. Then, 4 mmol  $\text{Y}(\text{NO}_3)_3$  were dissolved in the solution under continuous magnetic stirring at room temperature. Next, an aqueous solution containing 2.8 mmol of  $\text{NH}_4\text{VO}_3$  (12 mL), 3 mL of butylamine, and 9 mL of deionized water were added to the beaker. A copious white precipitate formed immediately, resulting from the formation of hydrophobic  $\text{YVO}_4$  nanocrystals. The white solids were collected by centrifugation and washed three times with ethanol.

**Synthesis of LaPO<sub>4</sub> Nanocrystals:** Butyric acid (5 mL), butylamine (5 mL), and ethanol (50 mL) were mixed in a 200-mL glass beaker. Then, 3 mmol La(NO<sub>3</sub>)<sub>3</sub> were dissolved in the solution under continuous magnetic stirring at room temperature. Next, an aqueous solution containing 3 mmol of NH<sub>4</sub>H<sub>2</sub>PO<sub>4</sub> (10 mL), 3 mL of butylamine, and 7 mL of deionized water were added to the beaker. A copious white precipitate formed immediately, resulting from the formation of hydrophobic LaPO<sub>4</sub> nanocrystals. The white solids were collected by centrifugation and washed three times with ethanol.

**Preparation of the colloidal glass film:** The colloidal glass film was synthesized through a two-stage process. First, a hydrophobic PDMS substrate was prepared by homogeneously mixing 1.2 g of silicone base agent with 0.12 g of cross-linker (10:1 mass ratio), followed by transferring into a 3.5-cm-diameter Petri dish and thermal curing at 65 °C for 12 hours to obtain a 5-mm-thick elastomeric substrate. Subsequently, 0.3 g of CaMoO<sub>4</sub>:Ln<sup>3+</sup> nanocrystals were dispersed in 3 mL of n-hexanol via ultrasonic agitation, and the resultant colloidal suspension was deposited onto the PDMS substrate. Upon complete evaporation of the solvent under ambient conditions, a mechanically stable transparent film formed on the PDMS surface, which could be cleanly delaminated as a freestanding membrane for optical characterization.

**Preparation of the PMMA Composite Film:** 90 mg of CaMoO<sub>4</sub>:15%Eu<sup>3+</sup> nanocrystals was dispersed in 3.0 mL of chloroform, followed by sonicating the solution for 10 min. Then, 270 mg of PMMA was added to the solution, followed by 20 min of sonication. The viscous solution was poured into a glass petri dish, and a composite film was obtained after solvent evaporation.

**Characterization:** X-ray diffraction (XRD) analysis was performed using a powder diffractometer (Bruker D8 Advance) with Cu-K $\alpha$  ( $\lambda = 1.5405 \text{ \AA}$ ) radiation. Transmission electron microscope (TEM) images were collected using a JEM-2100Plus (JEOL) at an acceleration voltage of 200 kV. Scanning electron microscope (SEM) images were obtained using a GeminiSEM 500 at an acceleration voltage of 5 kV. UV-vis reflectance spectra of film samples were measured with a UV-vis-near infrared spectrophotometer (LAMBDA 1050+).

Photoluminescence (PL) spectra of film samples were recorded using a fluorescence spectrometer (Edinburgh FLS1000).

**RL Measurement and X-ray Image Collection:** Radioluminescence (RL) spectra were recorded using a custom-built testing system with an integrating sphere equipped with a fiber-coupled NOVA2S-EX (Fuxiang Optics) spectrometer and an X-ray source (Moxtek, W target). Photographs of UV-excited and X-ray-induced emission were captured using a digital camera. RL images were recorded with a Sony ILCE-7M4 camera. To acquire the RL images, electronic chips were positioned between the X-ray source (30 kV, 50  $\mu$ A) and the scintillator films.

**Absorption coefficient calculation:** We extracted the attenuation coefficient of scintillation materials from XCOM: Photon Cross Sections Database (<https://physics.nist.gov/PhysRefData/Xcom/html/xcom1-t.html>). This online program provides total cross sections and partial cross sections, including Rayleigh scattering, Compton scattering, and photoelectric absorption.

**Modulation transfer function (MTF) measurements:** The MTF curve serves as a quantitative measure of an imaging system's ability to transfer object details into the resulting image. Spatial resolution is characterized as the spatial frequency at which the MTF equals 0.2. The inclined edge method was utilized to calculate the MTF. To begin, the edge spread function (ESF) was determined from an inclined edge profile. A sharp-edged aluminum sheet (approximately 1 mm thick) was placed on the prepared scintillator film. Under X-ray irradiation (20 kV, 30  $\mu$ A), the edge profile was captured, and the ESF was extracted. The corresponding line spread function (LSF) was obtained by differentiating the ESF, and the MTF was subsequently derived through the Fourier transform of the LSF. The calculation process adheres to the following formula:

$$MTF(\nu) = F(LSF(X)) = F\left(\frac{dESF(x)}{dx}\right)$$

where the  $\nu$  is spatial frequency,  $x$  is the position of pixels.

**Table S1. Scintillation characteristics of different materials.**

<b>Materials</b>	<b>T<sub>synthesis</sub> (°C)</b>	<b>Imaging resolution (lp/mm)</b>	<b>Refs.</b>
<b>NaLuF<sub>4</sub>: Tb/PDMS</b>	300	20	1
<b>NaGdF<sub>4</sub>:Ce,Tb/PMMA</b>	200	18.6	2
<b>YF<sub>3</sub>:Gd,Tb/PMMA</b>	90	16.8	3
<b>LaCsSiS<sub>4</sub>:Ce/EP</b>	850	8.2	4
<b>Cs<sub>3</sub>Cu<sub>2</sub>I<sub>5</sub>/PDMS</b>	RT	17	5
<b>Cs<sub>3</sub>Cu<sub>2</sub>I<sub>5</sub>/PMMA</b>	80	13.1	6
<b>CsPbBr<sub>3</sub> NCs/PMMA</b>	150	10	7
<b>CsPbBr<sub>3</sub>/PS</b>	90	175	8
<b>TEA<sub>2</sub>MnI<sub>4</sub> single crystal</b>	60	25	9
<b>Cs<sub>3</sub>Cu<sub>2</sub>I<sub>5</sub>:In single crystal</b>	550	18	10
<b>Cs<sub>3</sub>Cu<sub>2</sub>Cl<sub>5</sub> single crystal</b>	120	105	11
<b>(C<sub>8</sub>H<sub>20</sub>N)<sub>2</sub>Cu<sub>2</sub>Br<sub>4</sub> ceramics</b>	100	9.5	12
<b>CsPbBr<sub>3</sub>: Eu ceramics</b>	1200	15	13
<b>CaMoO<sub>4</sub>: 15%Eu<sup>3+</sup> colloidal glass</b>	<b>Room temperature</b>	<b>27.1</b>	<b>This work</b>

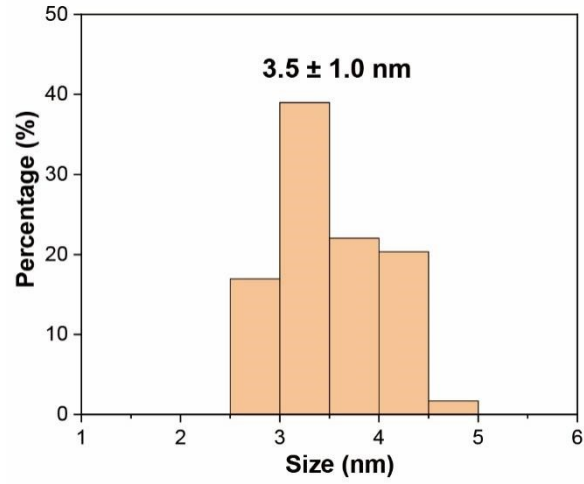


**Figure S1.** Size distribution of CaMoO<sub>4</sub>:15%Eu<sup>3+</sup> nanocrystals.

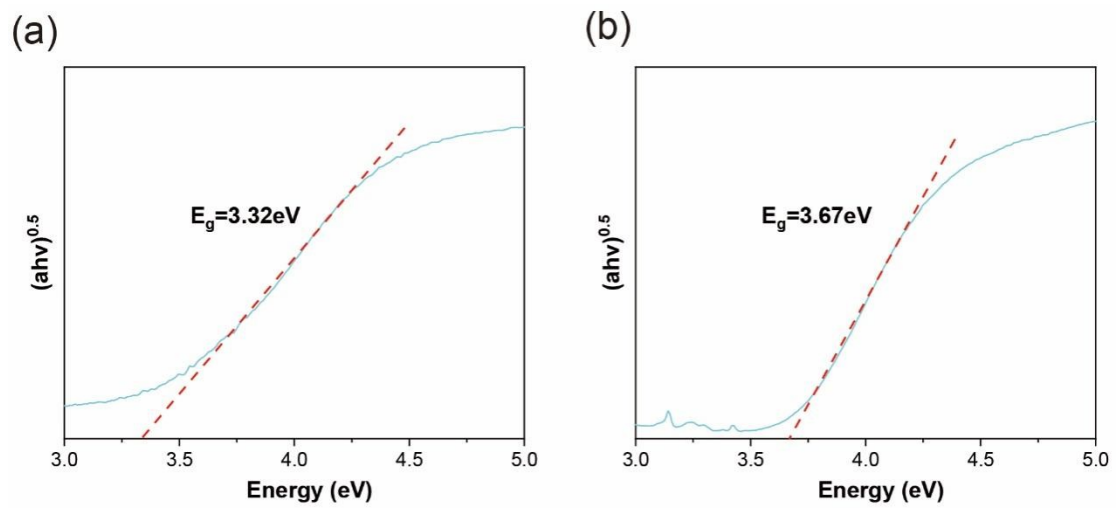


**Figure S2.** Optical band gaps of (a) CaMoO<sub>4</sub> nanocrystals and (b) CaMoO<sub>4</sub>:15%Eu<sup>3+</sup> nanocrystals.

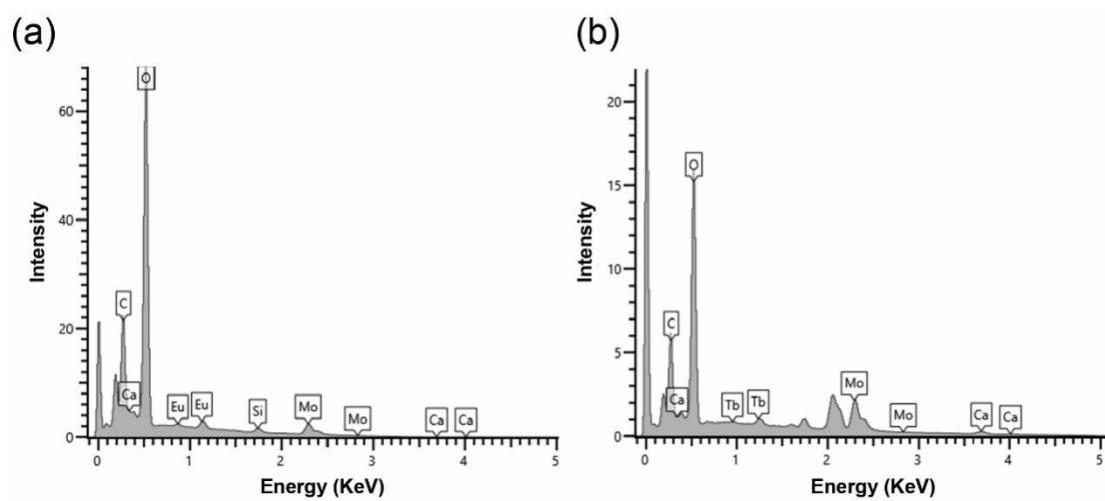


**Figure S3.** EDS of (a)  $\text{CaMoO}_4:15\%\text{Eu}^{3+}$  and (b)  $\text{CaMoO}_4:10\%\text{Tb}^{3+}$  colloidal glasses after solvent evaporation using n-hexanol.

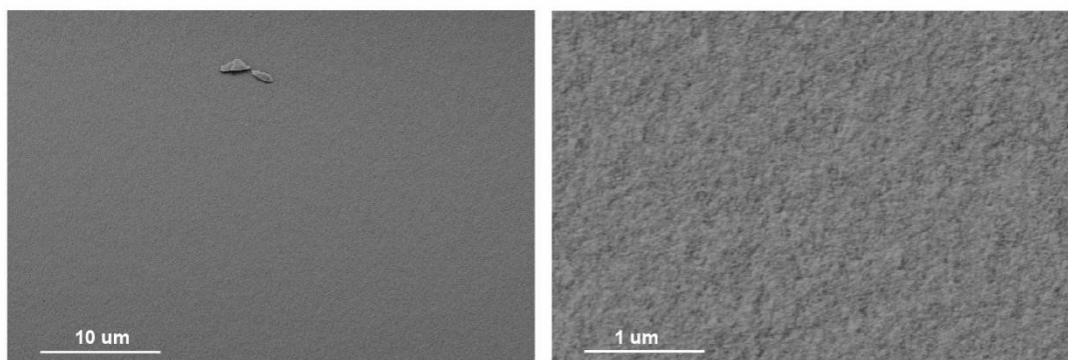


**Figure S4.** Cross-sectional and magnified SEM images of ethanol-derived  $\text{CaMoO}_4:15\%\text{Eu}^{3+}$  colloidal glass after solvent evaporation using ethanol.

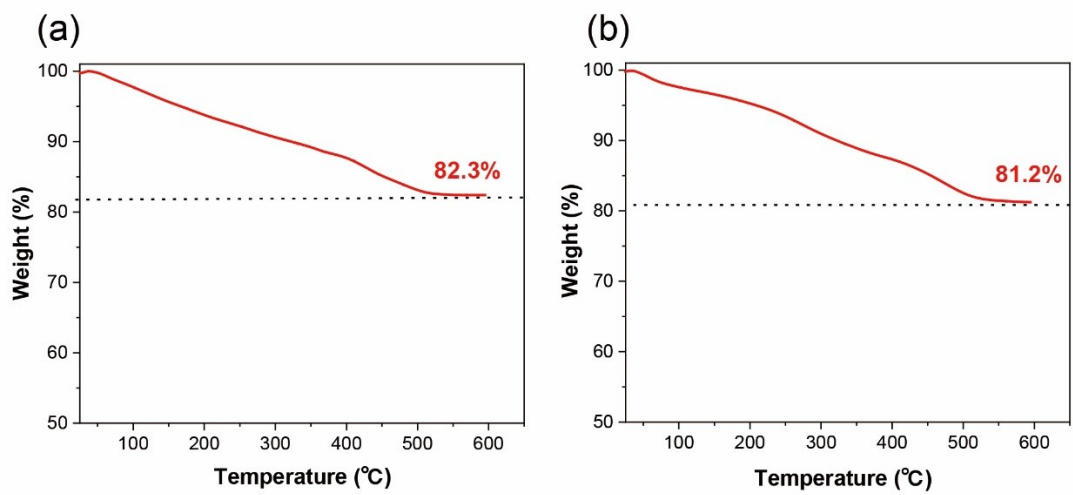


**Figure S5.** Thermogravimetric analysis (TGA) curve of  $\text{CaMoO}_4:15\%\text{Eu}^{3+}$  colloidal glasses after solvent evaporation using (a) ethanol and (b) n-hexanol.

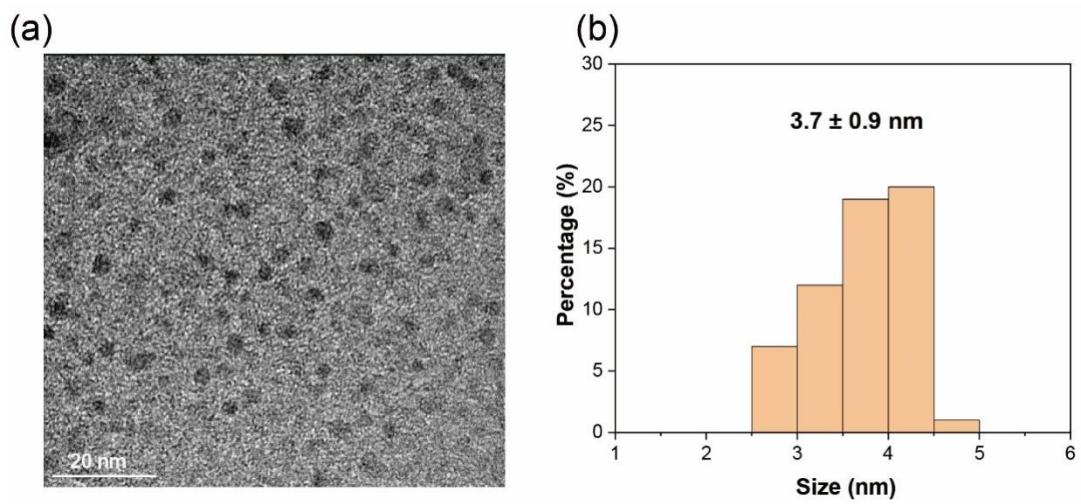


**Figure S6.** (a) TEM image and (b) Size distribution of  $\text{CaMoO}_4:10\%\text{Tb}^{3+}$  nanocrystals.

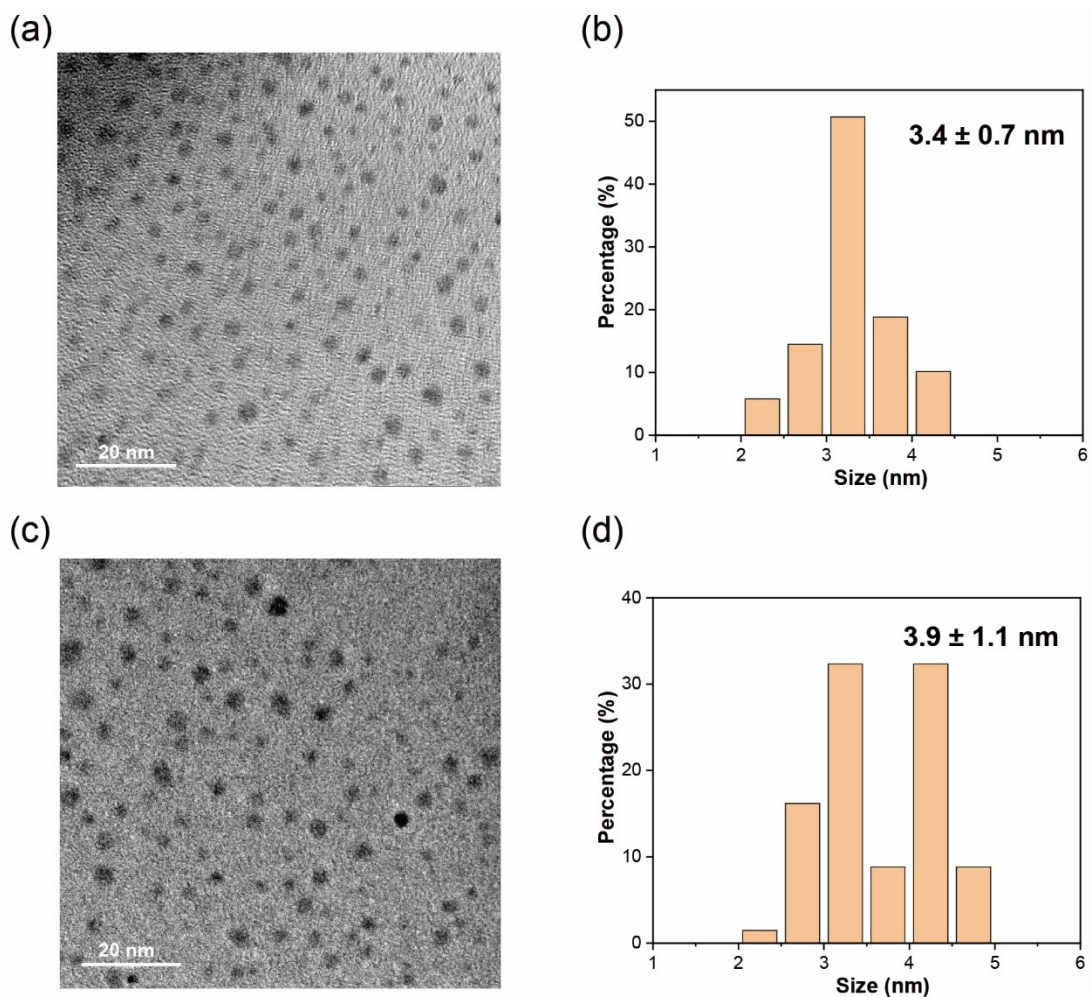


**Figure S7.** TEM images of (a)  $\text{YVO}_4$  nanocrystals and (c)  $\text{LaPO}_4$  nanocrystals. Size distribution of (b)  $\text{YVO}_4$  nanocrystals and (d)  $\text{LaPO}_4$  nanocrystals.

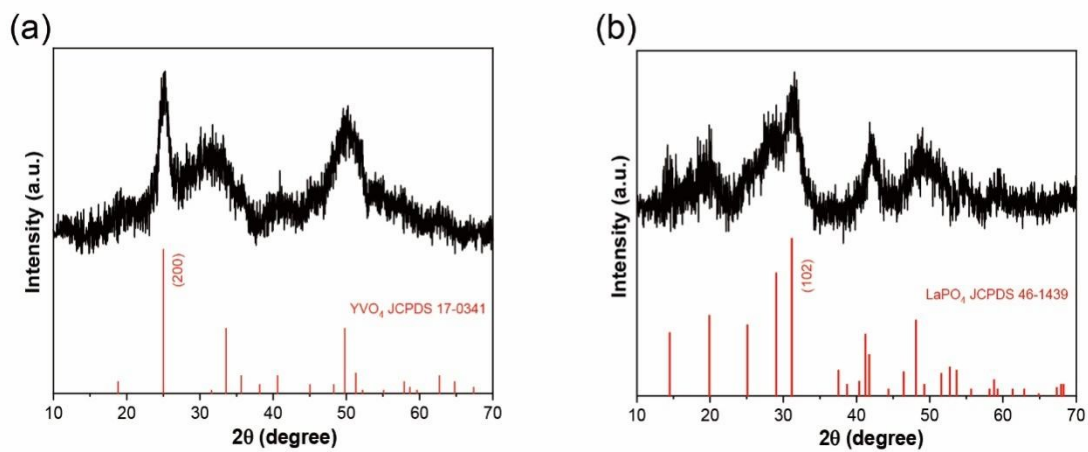


**Figure S8.** XRD patterns of (a)  $\text{YVO}_4$  and (b)  $\text{LaPO}_4$  colloidal glass after solvent evaporation using n-hexanol.

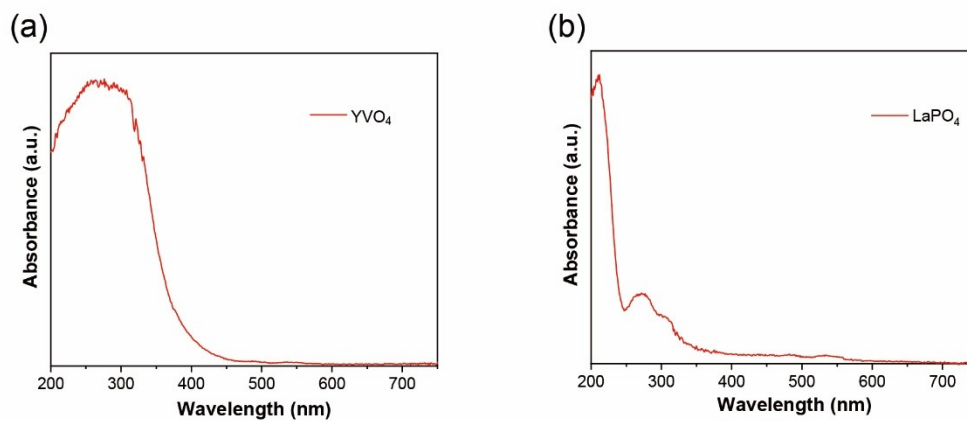


**Figure S9.** UV-vis diffuse reflectance spectra of (a)  $\text{YVO}_4$  and (b)  $\text{LaPO}_4$  colloidal glass after solvent evaporation using n-hexanol.

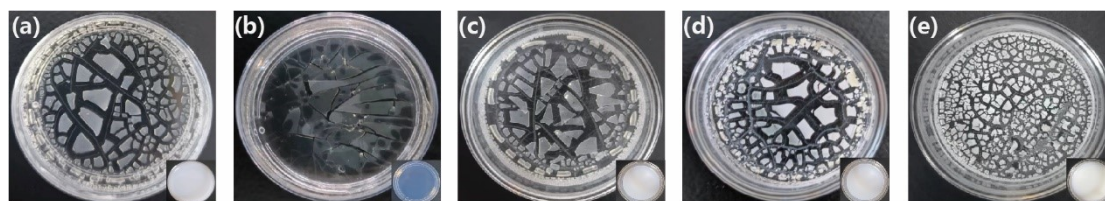


**Figure S10.** Photographs of  $\text{YVO}_4$  nanocrystal solids obtained after solvent evaporation using (a) ethanol, (b) n-hexanol, (c) chloroform, (d) toluene, (e) cyclohexane. Inset shows the optical images of the corresponding colloidal dispersion before solvent evaporation.

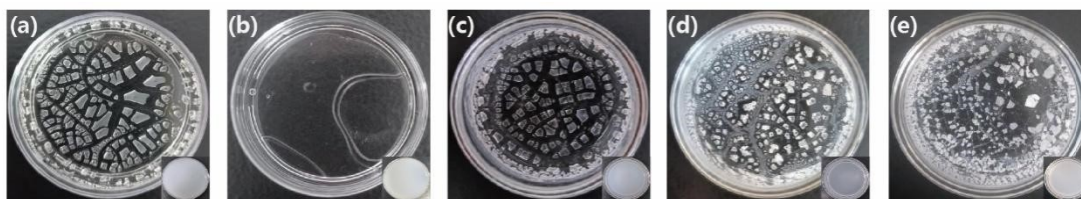


**Figure S11.** Photographs of  $\text{LaPO}_4$  nanocrystal solids obtained after solvent evaporation using (a) ethanol, (b) n-hexanol, (c) chloroform, (d) toluene, (e) cyclohexane. Inset shows the optical images of the corresponding colloidal dispersion before solvent evaporation.

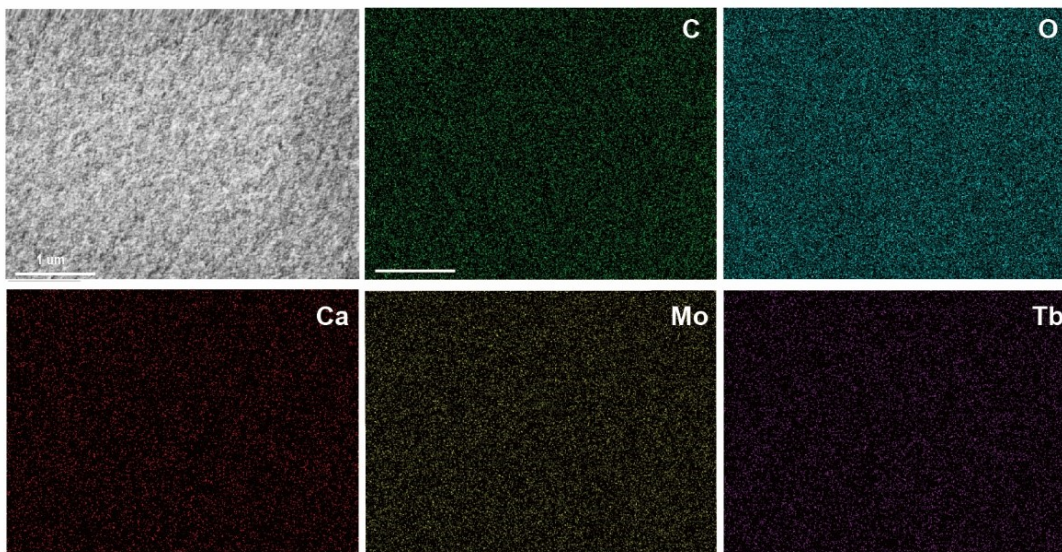


**Figure S12.** Cross-sectional SEM images and EDS mapping of the  $\text{CaMoO}_4:10\%\text{Tb}^{3+}$  colloidal glass film after solvent evaporation using n-hexanol.

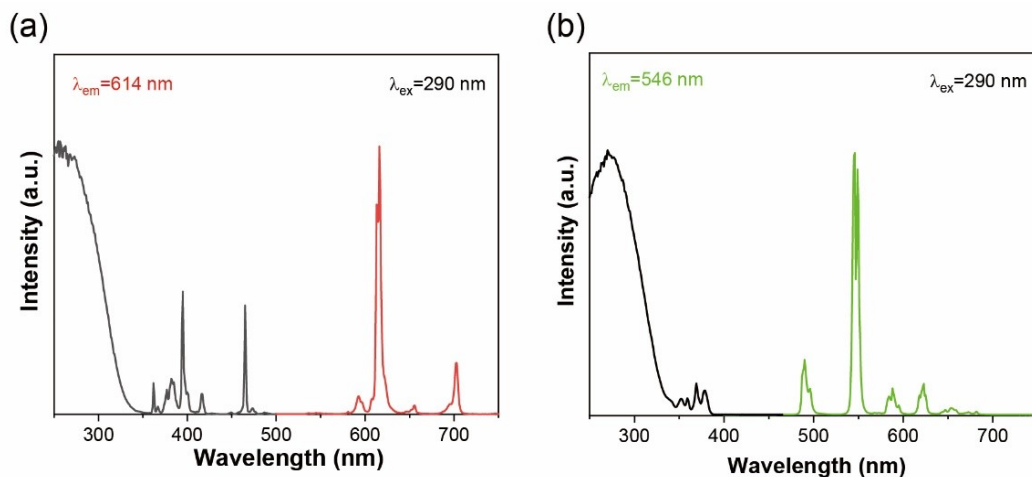


**Figure S13.** PL excitation and emission spectra of (a)  $\text{CaMoO}_4:15\%\text{Eu}^{3+}$  and (b)  $\text{CaMoO}_4:10\%\text{Tb}^{3+}$  colloidal glass film.

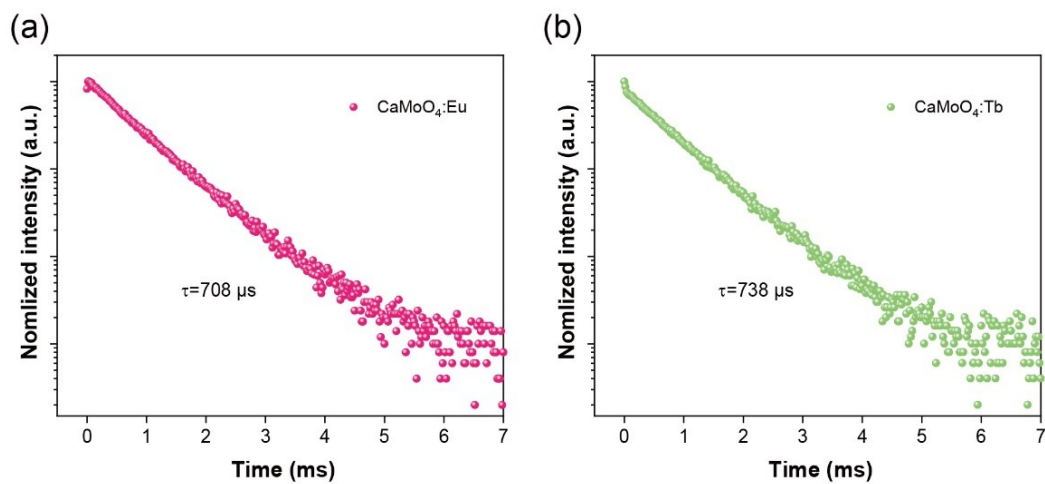


**Figure S14.** Time-resolved emission decay profiles of the (a)  $\text{CaMoO}_4:15\%\text{Eu}^{3+}$  and (b)  $\text{CaMoO}_4:10\%\text{Tb}^{3+}$  colloidal glass film.

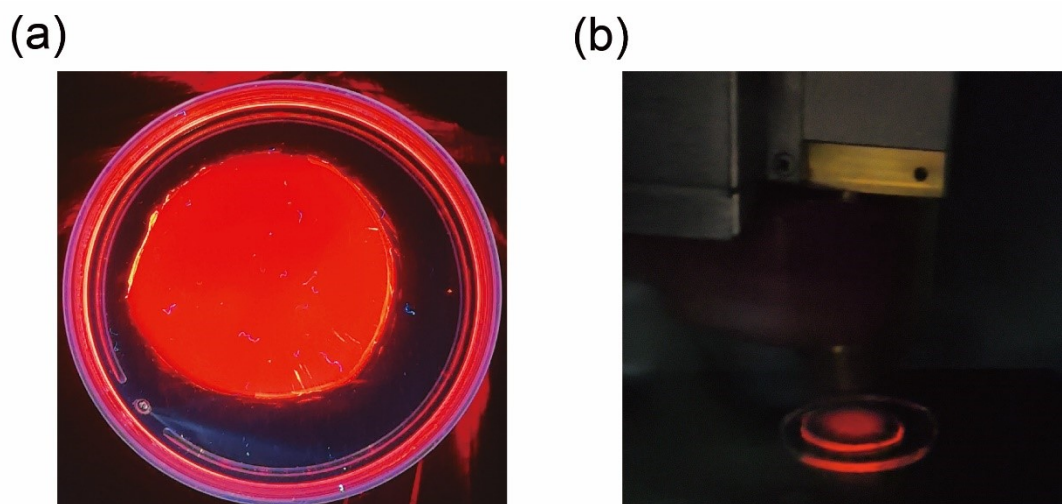


**Figure S15.** Photos of  $\text{CaMoO}_4:15\%\text{Eu}^{3+}$  colloidal glass film (a) under 365 nm UV light excitation and (b) under X-ray excitation.

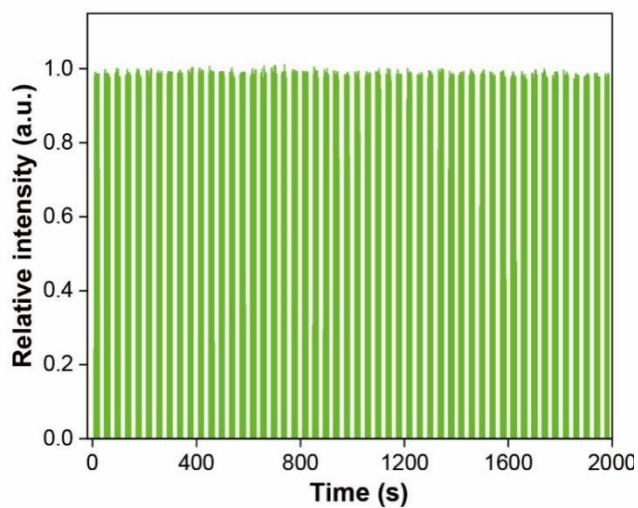


**Figure S16.** Radiation stability of the  $\text{CaMoO}_4:10\%\text{Tb}^{3+}$  colloidal glass film under cyclical test of X-ray irradiation (dose rate:  $550\mu\text{Gy/s}$ ).

## References

1. X. Ou, X. Qin, B. Huang, J. Zan, Q. Wu, Z. Hong, L. Xie, H. Bian, Z. Yi, X. Chen, Y. Wu, X. Song, J. Li, Q. Chen, H. Yang and X. Liu, *Nature*, 2021, **590**, 410-415.
2. J. Ma, W. Zhu, L. Lei, D. Deng, Y. Hua, Y. M. Yang, S. Xu and P. N. Prasad, *ACS Appl. Mater. Inter.*, 2021, **13**, 44596-44603.
3. Y. Ling, X. Zhao, P. Hao, Y. Song, J. Liu, L. Zhao, Y. Qian and C. Guo, *Chem. Eng. J.*, 2023, **476**.
4. L. Yang, Z. Li, L. He, J. Sun, J. Wang, Y. Wang, M. Li, Z. Zhu, X. Dai, S. X. Hu, F. Zhai, Q. Yang, Y. Tao, Z. Chai, S. Wang and Y. Wang, *Angew. Chem. Int. Ed.* 2023, **62**, e202306465.
5. Y. Zhou, X. Wang, T. He, H. Yang, C. Yang, B. Shao, L. Gutiérrez-Arzaluz, O. M. Bakr, Y. Zhang and O. F. Mohammed, *ACS Energy Lett.*, 2022, **7**, 844-846.
6. W. Zhou, X. Zhu, J. Yu, D. Mou, H. Li, L. Kong, T. Lang, L. Peng, W. Chen, X. Xu and B. Liu, *ACS Appl. Mater. Inter.* 2023, **15**, 38741-38749.
7. Y. Li, Y. Xu, Y. Yang, Z. Jia, H. Tang, J. B. Patel and Q. Lin, *Adv. Opt. Mater.*, 2023, **11**, 2300169.
8. R. Sun, Z. Wang, H. Wang, Z. Chen, Y. Yao, H. Zhang, Y. Gao, X. Hao, H. Liu and Y. Zhang, *ACS Appl. Mater. Inter.*, 2022, **14**, 36801-36806.
9. Z.-Z. Zhang, J.-H. Wei, J.-B. Luo, X.-D. Wang, Z.-L. He and D.-B. Kuang, *ACS Appl. Mater. Inter.*, 2022, **14**, 47913-47921.
10. Q. Wang, Q. Zhou, M. Nikl, J. Xiao, R. Kucerkova, A. Beitlerova, V. Babin, P. Prusa, V. Linhart, J. Wang, X. Wen, G. Niu, J. Tang, G. Ren and Y. Wu, *Adv. Opt. Mater.*, 2022, **10**, 2200304.
11. W. Xiang, D. Shen, X. Zhang, X. Li, Y. Liu and Y. Zhang, *ACS Appl. Mater. Inter.*, 2024, **16**, 4918-4924.
12. B. Su, J. Jin, K. Han and Z. Xia, *Adv. Funct. Mater.*, 2023, **33**, 2210735.
13. W. Ma, T. Jiang, Z. Yang, H. Zhang, Y. Su, Z. Chen, X. Chen, Y. Ma, W. Zhu, X. Yu, H. Zhu, J. Qiu, X. Liu, X. Xu and Y. Yang, *Adv. Sci.*, 2021, **8**, 2003728.